J. Fluid Mech. (1998), *vol.* 367, *pp.* 139–161. Printed in the United Kingdom

Interactions of a horizontal flexible membrane with oblique incident waves

By I. H. CHO† AND M. H. KIM

Department of Civil Engineering, Texas A & M University, College Station, TX 77843, USA

(Received 4 August 1997 and in revised form 27 February 1998)

The interaction of oblique monochromatic incident waves with a horizontal flexible membrane is investigated in the context of two-dimensional linear hydro-elastic theory. First, analytic diffraction and radiation solutions for a submerged impermeable horizontal membrane are obtained using an eigenfunction expansion method. Secondly, a multi-domain boundary element method (BEM) is developed to confirm the analytic solutions. The inner solution based on a discrete membrane dynamic model and simple-source distribution over the entire fluid boundaries is matched to the outer solution based on an eigenfunction expansion. The numerical solutions are in excellent agreement with the analytic solutions. The theoretical prediction was then compared to a series of experiments conducted in a two-dimensional wave tank at Texas A & M University. The measured reflection and transmission coefficients reasonably follow the trend of predicted values. Using the computer program developed, the performance of surface-mounted or submerged horizontal membrane wave barriers is tested with various system parameters and wave characteristics. It is found that the horizontal flexible membrane can be an effective wave barrier if properly designed.

1. Introduction

Most floating wave barriers are known to be ineffective in long waves unless their size is comparable to the pertinent wavelength. Therefore, to be a very effective wave barrier, the structural dimension has to be large and the resulting high construction cost has been a major obstruction for the realization of many floating-breakwater projects. During the past decade, there has been a gradual increase of interest in the use of flexible plates or membranes as alternative, effective, inexpensive wave barriers. In particular, the membrane is light and rapidly deployable, and thus it may be an ideal candidate as a portable temporary breakwater.

There have been many theoretical and experimental studies with regard to the performance of vertical flexible wave barriers. For example, the efficiency of a vertical-elastic-plate breakwater clamped at the seafloor was investigated by Lee & Chen (1990) and Williams, Geiger & McDougal (1991). Abul-Azm (1994) also showed that the efficiency of the elastic-beam breakwater can be improved by tuning two vertical plates. On the other hand, the performance of a vertical-screen membrane breakwater, which is equivalent to the tensioned elastic-beam breakwater with zero bending rigidity, was investigated by Thomson *et al.* (1992), Aoki, Liu & Sawaragi (1994), Kim & Kee (1996), Kee & Kim (1997), and Williams (1996). Using the linear wave theory and membrane-

† Current address: Korea Research Institute of Ships & Ocean Engineering, Daejon, Korea.

motion equation, Kim & Kee (1996) and Kee & Kim (1997) showed that almost complete reflection was possible by a vertically flexible membrane despite appreciable sinusoidal motions, which tend to generate only exponentially decaying local (evanescent) waves in the lee side. The theory was compared favourably with 2-D tank experiments (Kim *et al*. 1996). This interesting phenomenon can also be partly explained by a classical wavemaker theory (Dean & Dalrymple 1991).

One of the major problems associated with the use of a flexible vertical screen is the expected large wave loading and possible blockage of currents. In view of this, the possibility of using an alternative horizontal membrane, which has not been studied in the open literature, is investigated in this paper. In particular, the submerged horizontal membrane does not hamper the seascape and also allows the passage of ships and currents. Since the horizontal membrane does not directly block incoming waves, the diffracted and radiated waves including various elastic modes have to be properly tuned to be an effective wave barrier. The formulation for the interaction of a submerged horizontal membrane with waves is in general more complicated than the vertical-membrane case. Siew & Hurley (1977) and McIver (1985), for instance, studied the diffraction of linear waves by a submerged horizontal rigid flat plate. They showed that it can reflect significant amounts of incident wave energy at certain wave frequencies. In the present study, it is shown that the overall wave-blocking efficiency can be greatly improved by using horizontal flexible membranes instead of rigid plates. The relevant hydro-elastic theory is formulated in §2 for arbitrary incident wave angles.

In §3, a multi-domain boundary element method (BEM) is independently developed to confirm the analytic solutions derived in the preceding section. The computational domain is decomposed into inner and outer domains. Inside the inner region, a simple-source (modified Bessel function of the second kind) distribution and a discrete membrane dynamic model are used. For the outer region, an eigenfunction expansion method is used. The inner solution is matched at vertical matching boundaries to the outer solution based on the continuity of pressure and normal velocity. The numerical results compare excellently with the analytic solutions. It is also shown that both analytic and numerical solutions satisfy energy conservation. The present hydroelastic theory is also verified by a series of experiments conducted in a two-dimensional wave tank at Texas A & M University, which is summarized in §4. It is seen that the wave-blocking performance by a horizontal flexible membrane can be reasonably predicted by the present linear hydro-elastic theory.

Finally, in §5, the performance of various designs of horizontal-membrane wave barriers is studied for a variety of wave conditions or water depths. It is shown that the system can be highly efficient if it is properly designed and the high-performance region can be controlled by changing relevant design parameters. The results are summarized and concluding remarks are given in §6.

2. Mathematical formulation and analytic solutions

We consider the interaction of a horizontal membrane wave barrier with monochromatic oblique incident waves. Cartesian axes are chosen with the (x, z)-axes in the mean free surface and the y-axis pointing vertically upwards. The water depth is denoted by h and the submergence depth of the membrane by d. It is assumed that both ends of the membrane are fixed at $x = \pm a$, and a uniform tension T is applied on the membrane in the x-direction (see figure 1*a*). It is also assumed that the fluid is incompressible and inviscid, and the wave and membrane motions are small so that

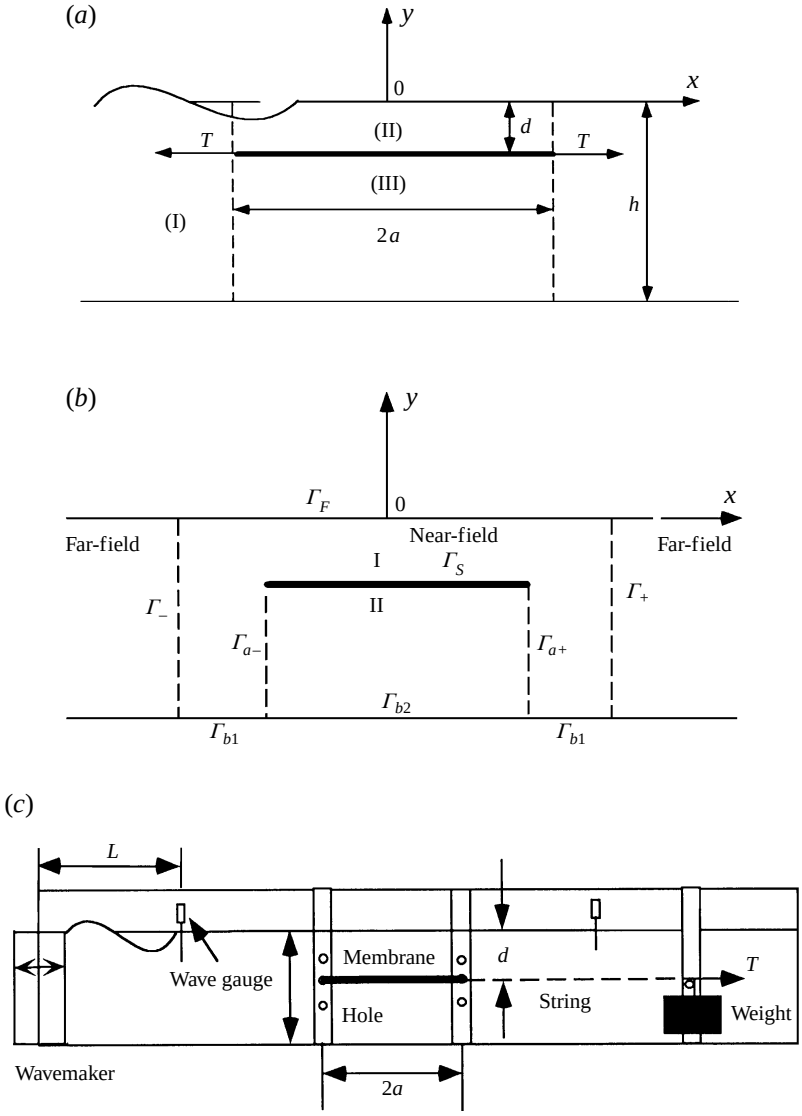

FIGURE 1. (*a*) Definition sketch for horizontal impermeable flexible membrane. (*b*) Integration domains for a numerical solution. (*c*) Experimental set-up of a submerged horizontal membrane breakwater.

linear potential theory can be used. The fluid particle velocity can then be described by the gradient of a velocity potential $\Phi(x, y, z, t)$. The wave profile periodically changes in the z-direction; thus the variation in the z-direction can be separated out. Then, a two-dimensional analysis can be applied at each section. Assuming harmonic motion of frequency ω, the velocity potential can be written as $\Phi(x, y, z, t) = \mathrm{Re}[\phi(x, y)\,\mathrm{e}^{\mathrm{i}k_z z - \mathrm{i}\omega t}]$, where $k_z = k_1 \sin\theta$ is the z-component wavenumber and θ is the heading of incident waves with respect to the x-axis. Similarly, the vertical displacement of membrane can be written as

$$\zeta(x, z, t) = \mathrm{Re}[\xi(x)\,\mathrm{e}^{\mathrm{i}k_z z - \mathrm{i}\omega t}], \tag{2.1}$$

where $\xi(x)$ is the complex displacement of membrane.

The velocity potential ϕ satisfies the modified Helmholtz equation

$$\frac{\partial^2\phi}{\partial x^2}+\frac{\partial^2\phi}{\partial y^2}-k_1^2\sin^2\theta\phi=0 \text{ in the fluid,} \tag{2.2}$$

with the following boundary conditions:

$$\frac{\partial\phi}{\partial y}-\nu\phi=0 \quad \text{on} \quad y=0 \qquad \nu=\frac{\omega^2}{g}\ , \tag{2.3}$$

$$\frac{\partial\phi}{\partial y}=0 \quad \text{on} \quad y=-h, \tag{2.4}$$

$$\lim_{x\to\pm\infty}\ \frac{\partial\phi}{\partial x}\mp \mathrm{i}k_1\cos\theta\phi\ =0, \tag{2.5}$$

$$\frac{\partial\phi}{\partial y}=-\mathrm{i}\omega\xi \quad \text{on} \quad y=-d, \quad -a\leqslant x\leqslant a. \tag{2.6}$$

The complex displacement of the membrane can be expanded in terms of a set of its natural modes:

$$\xi(x)=\sum_{l=1}^{\infty}\varsigma_l f_l(x), \tag{2.7}$$

where ς_l is the unknown complex modal amplitude corresponding to the lth mode. The modal functions and eigenvalues of the membrane satisfying the membrane equation and the end condition are given by

$$f_l(x)=\begin{cases} f_l^S(x)=\cos\dfrac{\lambda_l^S x}{a}, \quad \lambda_l^S=\dfrac{[2(l-1)+1]\pi}{2} \quad (l=1,2,3,\ldots) \\ f_l^A(x)=\sin\dfrac{\lambda_l^A x}{a}, \quad \lambda_l^A=l\pi \quad (l=1,2,3,\ldots), \end{cases} \tag{2.8}$$

where the superscripts S and A denote symmetric and asymmetric modes about $x=0$, respectively. The modal functions given in equation (2.8) are orthogonal to each other in the interval $[-a,a]$:

$$\int_{-a}^{a} f_i(x)f_j(x)\,\mathrm{d}x=\begin{matrix} a, & i=j \\ 0, & i\neq j. \end{matrix} \tag{2.9}$$

Including all the flexible membrane modes, the complex potential $\phi(x,y)$ can be expressed in the form

$$\left.\begin{aligned} \phi(x,y)&=\phi_D(x,y)+\sum_{l=1}^{\infty}\varsigma_l\phi_{lR}(x,y), \\ \phi_D(x,y)&=\phi_I(x,y)+\phi_S(x,y), \end{aligned}\right\} \tag{2.10}$$

where ϕ_D is the diffraction potential and ϕ_S,ϕ_{lR} denote the scattering and radiation potential, respectively. The incident wave potential ϕ_I is given by

$$\phi_I(x,y)=-\frac{\mathrm{i}gA}{\omega}\frac{\cosh k_1(y+h)}{\cosh k_1 h}\mathrm{e}^{\mathrm{i}k_1\cos\theta x}, \tag{2.11}$$

where g is the gravitational acceleration, A is the wave amplitude, and k_1 is the wavenumber satisfying the usual dispersion relation

$$\frac{\omega^2}{g} = k_1 \tanh k_1 h. \tag{2.12}$$

From now on, A is set to be unity for convenience.

2.1. *Diffraction problem*

The diffraction potential ϕ_D satisfies equation (2.2)–(2.5) and the following membrane boundary condition:

$$\frac{\partial \phi_D}{\partial y} = 0 \quad \text{on} \quad y = -d, \quad -a \leqslant x \leqslant a. \tag{2.13}$$

In the following, the symmetry of the fluid and membrane is used by splitting ϕ_D into symmetric and asymmetric parts.

$$\phi_D(x, y) = \phi_D^S(x, y) + \phi_D^A(x, y), \tag{2.14a}$$

where

$$\left.\begin{aligned} &\phi_D^S(-x, y) = \phi_D^S(x, y), \quad \frac{\partial \phi_D^S}{\partial x} = 0 \\ &\phi_D^A(-x, y) = -\phi_D^A(x, y), \quad \phi_D^A = 0 \end{aligned}\right\} \quad \text{on} \quad x = 0. \tag{2.14b}$$

The fluid domain is divided into three regions, as shown in figure 1(*a*). Region (I) is defined by $x \leqslant -a$, $-h < y < 0$, region (II) by $|x| \leqslant a$, $-d < y < 0$ and region (III) by $|x| \leqslant a$, $-h < y < -d$.

The symmetric diffraction potentials in the three fluid regions are written as

$$\left.\begin{aligned} \phi_D^{S(1)} &= -\frac{\mathrm{i}g}{\omega}\left[\tfrac{1}{2}\mathrm{e}^{-\alpha_{10}x} f_{10}(y) + \sum_{n=0}^{\infty} a_n^S \mathrm{e}^{\alpha_{1n}(x+a)} f_{1n}(y)\right], \\ \phi_D^{S(2)} &= -\frac{\mathrm{i}g}{\omega} \sum_{n=0}^{\infty} b_n^S \cosh(\alpha_{2n} x) f_{2n}(y), \\ \phi_D^{S(3)} &= -\frac{\mathrm{i}g}{\omega} \sum_{n=0}^{\infty} c_n^S \cosh(\alpha_{3n} x) f_{3n}(y), \end{aligned}\right\} \tag{2.15a}$$

where

$$\left.\begin{aligned} \alpha_{1n} &= \begin{cases} -\mathrm{i}k_1 \cos\theta, & n = 0 \\ (k_1^2 \sin^2\theta + k_{1n}^2)^{1/2}, & n \geqslant 1, \end{cases} \\ \alpha_{2n} &= \begin{cases} -\mathrm{i}k_2 (1 - (k_1/k_2)^2 \sin^2\theta)^{1/2}, & n = 0 \\ (k_1^2 \sin^2\theta + k_{2n}^2)^{1/2}, & n \geqslant 1, \end{cases} \\ \alpha_{3n} &= (k_1^2 \sin^2\theta + k_{3n}^2)^{1/2}, \quad n \geqslant 0. \end{aligned}\right\} \tag{2.15b}$$

The eigenfunctions $f_{1n}(y)$, $f_{2n}(y)$, and $f_{3n}(y)$ are given by

$$f_{1n}(y) = \begin{cases} \cosh k_1(y+h)/\cosh k_1 h, & n = 0 \\ \cos k_{1n}(y+h)/\cos k_{1n} h, & n \geqslant 1. \end{cases} \tag{2.16}$$

$$f_{2n}(y) = \begin{cases} \cosh k_2(y+d)/\cosh k_2 d, & n = 0, \\ \cos k_{2n}(y+d)/\cos k_{2n} d, & n \geqslant 1. \end{cases} \tag{2.17}$$

$$f_{3n}(y) = \cos k_{3n}(y+h)/\cos k_{3n}(h-d), \quad n \geqslant 0. \tag{2.18}$$

The eigenvalues k_{1n}, k_{2n}, k_{3n} are the solutions of the following equations:

$$\left.\begin{aligned} k_1 \tanh k_1 h &= \frac{\omega^2}{g}, && n = 0, \\ k_{1n} \tan k_{1n} h &= -\frac{\omega^2}{g}, && n \geqslant 1. \end{aligned}\right\} \tag{2.19}$$

$$\left.\begin{aligned} k_2 \tanh k_2 d &= \frac{\omega^2}{g}, && n = 0, \\ k_{2n} \tan k_{2n} d &= -\frac{\omega^2}{g}, && n \geqslant 1. \end{aligned}\right\} \tag{2.20}$$

$$k_{3n} = n\pi/(h-d), \quad n \geqslant 0. \tag{2.21}$$

The unknown coefficients a_n^S, b_n^S, c_n^S $(n = 0, 1, 2, \ldots)$ can then be determined by invoking the continuity of potential and horizontal velocity at $x = -a$. The continuity of ϕ_D^S at $x = -a$ requires that

$$\tfrac{1}{2} e^{\alpha_{10} a} f_{10}(y) + \sum_{n=0}^{\infty} a_n^S f_{1n}(y) = \begin{cases} \displaystyle\sum_{n=0}^{\infty} b_n^S \cosh(\alpha_{2n} a) f_{2n}(y), & -d \leqslant y \leqslant 0 \\ \displaystyle\sum_{n=0}^{\infty} c_n^S \cosh(\alpha_{3n} a) f_{3n}(y), & -h \leqslant y \leqslant -d. \end{cases} \tag{2.22a, b}$$

Multiplying (2.22*a*) by $f_{2m}(y)$ and integrating with respect to y over $[-d, 0]$, we obtain

$$b_m^S \cosh(\alpha_{2m} a) N_m^{(2)} = \tfrac{1}{2} e^{\alpha_{10} a} C_{m0} + \sum_{n=0}^{\infty} a_n^S C_{mn}, \tag{2.23a}$$

where

$$\int_{-d}^{0} f_{2n}(y) f_{2m}(y)\, dy = \begin{cases} N_m^{(2)}, & m = n \\ 0, & m \neq n, \end{cases} \qquad N_m^{(2)} = \frac{d}{2\cos^2(k_{2m} d)} \left[1 + \frac{\sin(2k_{2m} d)}{2k_{2m} d}\right], \tag{2.23b}$$

$$C_{mn} = \int_{-d}^{0} f_{1n}(y) f_{2m}(y)\, dy,$$

$$= [2\cos(k_{1n} h)\cos(k_{2m} d)]^{-1} \left[\frac{2k_{1n} \sin[k_{1n}(h-d)]}{k_{2m}^2 - k_{1n}^2} + \frac{\sin(dk_{2m} + hk_{1n})}{k_{2m} + k_{1n}} + \frac{\sin(dk_{2m} - hk_{1n})}{k_{2m} - k_{1n}}\right]. \tag{2.23c}$$

Here k_{1n}, k_{2n} are real for $n > 0$, while k_{10}, k_{20} are imaginary and defined by $k_{10} = -ik_1$, $k_{20} = -ik_2$. If we multiply (2.22*b*) by $f_{3m}(y)$ and integrate with respect to y from $-h$ to $-d$, the following equation can be obtained:

$$c_m^S \cosh(\alpha_{3m} a) N_m^{(3)} = \tfrac{1}{2} e^{\alpha_{10} a} D_{m0} + \sum_{n=0}^{\infty} a_n^S D_{mn}, \tag{2.24a}$$

where

$$\int_{-h}^{-d} f_{3n}(y) f_{3m}(y)\,\mathrm{d}y = \begin{cases} N_m^{(3)}, & m = n \\ 0, & m \neq n, \end{cases} \qquad N_m^{(3)} = \begin{cases} (h-d), & m = 0 \\ \tfrac{1}{2}(h-d), & m \neq 0, \end{cases} \tag{2.24b}$$

$$D_{mn} = \int_{-h}^{-d} f_{1n}(y) f_{3m}(y)\,\mathrm{d}y,$$

$$= [2\cos(k_{1n}h)\cos\{k_{3m}(h-d)\}]^{-1} \left\{ \frac{\sin[(k_{3m}+k_{1n})(h-d)]}{k_{3m}+k_{1n}} + \frac{\sin[(k_{3m}-k_{1n})(h-d)]}{k_{3m}-k_{1n}} \right\}. \tag{2.24c}$$

On the other hand, the continuity of $\partial\phi_D^S/\partial x$ at $x = -a$ gives

$$-\tfrac{1}{2}\alpha_{10}\mathrm{e}^{\alpha_{10}a} f_{10}(y) + \sum_{n=0}^{\infty} \alpha_{1n} a_n^S f_{1n}(y) = \begin{cases} -\sum_{n=0}^{\infty} \alpha_{2n} b_n^S \sinh(\alpha_{2n}a) f_{2n}(y), & -d \leqslant y \leqslant 0. \\ -\sum_{n=0}^{\infty} \alpha_{3n} c_n^S \sinh(\alpha_{3n}a) f_{3n}(y), & -h \leqslant y \leqslant -d. \end{cases} \tag{2.25}$$

Multiplying both sides of equation (2.25) by $f_{1m}(y)$ and integrating with respect to y from $-h$ to 0, we obtain

$$\alpha_{1m} a_m^S N_m^{(1)} = -\sum_{n=0}^{\infty} \alpha_{2n} b_n^S \sinh(\alpha_{2n}a) C_{nm} - \sum_{n=0}^{\infty} \alpha_{3n} c_n^S \sinh(\alpha_{3n}a) D_{nm}, \tag{2.26a}$$

where

$$\int_{-h}^{0} f_{1n}(y) f_{1m}(y)\,\mathrm{d}y = \begin{cases} N_m^{(1)}, & m = n \\ 0, & m \neq n, \end{cases} \qquad N_m^{(1)} = \frac{h}{2\cos^2(k_{1m}h)} \left\{ 1 + \frac{\sin(2k_{1m}h)}{2k_{1m}h} \right\}. \tag{2.26b}$$

The final matrix equation for a_m^S can then be obtained by substituting equation (2.23) and (2.24) into equation (2.26*a*):

$$\left.\begin{aligned} a_0^S + \sum_{k=0}^{\infty} \frac{F_{0k}^S}{\alpha_{10} N_0^{(1)}} a_k^S &= -\tfrac{1}{2}\mathrm{e}^{\alpha_{10}a} \left\{ \frac{F_{00}^S}{\alpha_{10} N_0^{(1)}} - 1 \right\}, & m = 0, \\ a_m^S + \sum_{k=0}^{\infty} \frac{F_{mk}^S}{\alpha_{1m} N_m^{(1)}} a_k^S &= -\tfrac{1}{2}\mathrm{e}^{\alpha_{10}a} \frac{F_{m0}^S}{\alpha_{1m} N_m^{(1)}}, & m = 1, 2, 3, \ldots, \end{aligned}\right\} \tag{2.27a}$$

where

$$F_{mk}^S + \sum_{n=0}^{\infty} \frac{\alpha_{2n}\tanh(\alpha_{2n}a)\, C_{nm} C_{nk}}{N_n^{(2)}} + \sum_{n=0}^{\infty} \frac{\alpha_{3n}\tanh(\alpha_{3n}a)\, D_{nm} D_{nk}}{N_n^{(3)}}. \tag{2.27b}$$

By solving the above simultaneous algebraic equations, the unknown constants a_n^S can be determined. Subsequently, the other unknown constants b_n^S, c_n^S can be derived from equations (2.22) and (2.23) as follows:

$$b_n^S = \frac{\tfrac{1}{2}\mathrm{e}^{\alpha_{10}a} C_{n0} + \sum_{k=0}^{\infty} a_k^S C_{nk}}{\cosh(\alpha_{2n}a) N_n^{(2)}}, \quad c_n^S = \frac{\tfrac{1}{2}\mathrm{e}^{\alpha_{10}a} D_{n0} + \sum_{k=0}^{\infty} a_k^S D_{nk}}{\cosh(\alpha_{3n}a) N_n^{(3)}}, \quad n \geqslant 0. \tag{2.28}$$

Similarly, the asymmetric diffraction potentials in the three fluid regions are written as

$$\left.\begin{aligned}\phi_D^{A(1)} &= -\frac{\mathrm{i}g}{\omega}\left[\tfrac{1}{2}\mathrm{e}^{-\alpha_{10}x}f_{10}(y)+\sum_{n=0}^{\infty}a_n^A\,\mathrm{e}^{\alpha_{1n}(x+a)}f_{1n}(y)\right],\\ \phi_D^{A(2)} &= -\frac{\mathrm{i}g}{\omega}\sum_{n=0}^{\infty}b_n^A\sinh(\alpha_{2n}x)f_{2n}(y),\\ \phi_D^{A(3)} &= -\frac{\mathrm{i}g}{\omega}\sum_{n=0}^{\infty}c_n^A\sinh(\alpha_{3n}x)f_{3n}(y).\end{aligned}\right\} \tag{2.29}$$

The unknown coefficients a_n^A, b_n^A, c_n^A $(n=0,1,2,\ldots)$ can be determined in a similar manner by applying the continuity of potentials and horizontal velocities on $x=-a$:

$$\left.\begin{aligned}a_0^A+\sum_{k=0}^{\infty}\frac{F_{0k}^A}{\alpha_{10}N_0^{(1)}}a_k^A &= -\tfrac{1}{2}\mathrm{e}^{\alpha_{10}a}\left[\frac{F_{00}^A}{\alpha_{10}N_0^{(1)}}-1\right], \quad m=0,\\ a_m^A+\sum_{k=0}^{\infty}\frac{F_{mk}^A}{\alpha_{1m}N_m^{(1)}}a_k^A &= -\tfrac{1}{2}\mathrm{e}^{\alpha_{10}a}\frac{F_{m0}^A}{\alpha_{1m}N_m^{(1)}}, \quad m=1,2,3,\ldots,\end{aligned}\right\} \tag{2.30a}$$

where

$$F_{mk}^A=\sum_{n=0}^{\infty}\frac{\alpha_{2n}\coth(\alpha_{2n}a)\,C_{nm}\,C_{nk}}{N_n^{(2)}}+\sum_{n=0}^{\infty}\frac{\alpha_{3n}\coth(\alpha_{3n}a)\,D_{nm}\,D_{nk}}{N_n^{(3)}}. \tag{2.30b}$$

The remaining unknown coefficients b_n^A and c_n^A can then be determined from

$$b_n^A=-\frac{\tfrac{1}{2}\mathrm{e}^{\alpha_{10}a}C_{n0}+\sum_{k=0}^{\infty}a_k^A\,C_{nk}}{\sinh(\alpha_{2n}a)N_n^{(2)}}, \quad c_n^A=-\frac{\tfrac{1}{2}\mathrm{e}^{\alpha_{10}a}D_{n0}+\sum_{k=0}^{\infty}a_4^A\,D_{nk}}{\sinh(\alpha_{3n}a)N_n^{(3)}}, \quad n\geqslant 0. \tag{2.31}$$

2.2. *Radiation problem*

The radiation potential of each mode, ϕ_{lR}, is governed by (2.2)–(2.5) and the following body-boundary condition:

$$\frac{\partial\phi_{lR}}{\partial y}=-\mathrm{i}\omega f_l(x) \quad \text{on} \quad y=-d, \quad -a\leqslant x\leqslant a. \tag{2.32}$$

For simplicity, we split ϕ_{lR} into symmetric and asymmetric parts as in the diffraction problem:

$$\phi_{lR}(x,y)=\phi_{lR}^S(x,y)+\phi_{lR}^A(x,y). \tag{2.33}$$

The radiation potentials in regions (II) and (III) can be represented by the sum of a homogeneous solution and a particular solution. The homogeneous solutions look similar to those considered in the diffraction problem. The symmetric radiation potentials in each region can be written as

$$\left.\begin{aligned}\phi_{lR}^{S(1)} &= -\frac{\mathrm{i}g}{\omega}\sum_{n=0}^{\infty}a_{ln}^S\,\mathrm{e}^{\alpha_{1n}(x+a)}f_{1n}(y),\\ \phi_{lR}^{S(2)} &= -\frac{\mathrm{i}g}{\omega}\left[\sum_{n=0}^{\infty}b_{ln}^S\cosh(\alpha_{2n}x)f_{2n}(y)+\frac{\mathrm{i}\omega}{g}\tilde{\phi}_{lR}^{S(2)}(x,y)\right],\\ \phi_{lR}^{S(3)} &= -\frac{\mathrm{i}g}{\omega}\left[\sum_{n=0}^{\infty}c_{ln}^S\cosh(\alpha_{3n}x)f_{3n}(y)+\frac{\mathrm{i}\omega}{g}\tilde{\phi}_{lR}^{S(3)}(x,y)\right].\end{aligned}\right\} \tag{2.34}$$

The symmetric radiation potentials can be expressed in a similar manner:

$$\left.\begin{aligned}
\phi_{lR}^{A(1)} &= -\frac{\mathrm{i}g}{\omega}\sum_{n=0}^{\infty} a_{ln}^{A}\,\mathrm{e}^{\alpha_{1n}(x+a)} f_{1n}(y),\\
\phi_{lR}^{A(2)} &= -\frac{\mathrm{i}g}{\omega}\sum_{n=0}^{\infty} b_{ln}^{A}\sinh(\alpha_{2n}x) f_{2n}(y)+\frac{\mathrm{i}\omega}{g}\tilde{\phi}_{lR}^{A(2)}(x,y)\ ,\\
\phi_{lR}^{A(3)} &= -\frac{\mathrm{i}g}{\omega}\sum_{n=0}^{\infty} c_{ln}^{A}\sinh(\alpha_{3n}x) f_{3n}(y)+\frac{\mathrm{i}\omega}{g}\tilde{\phi}_{lR}^{A(3)}(x,y)\ .
\end{aligned}\right\} \tag{2.35}$$

The particular solutions in regions (II) and (III) satisfying the inhomogeneous body-boundary condition can be obtained as

$$\tilde{\phi}_{lR}^{S(2)}(x,y)=\frac{-\mathrm{i}\omega\cos(\lambda_l^S x/a)\,[m_1\cosh(m_1 y)+\nu\sinh(m_1 y)]}{m_1[-m_1\sinh(m_1 d)+\nu\cosh(m_1 d)]}, \tag{2.36}$$

$$\tilde{\phi}_{lR}^{A(2)}(x,y)=\frac{-\mathrm{i}\omega\sin(\lambda_l^A x/a)\,[m_2\cosh(m_2 y)+\nu\sinh(m_2 y)]}{m_2[-m_2\sinh(m_2 d)+\nu\cosh(m_2 d)]}, \tag{2.37}$$

$$\tilde{\phi}_{lR}^{S(3)}(x,y)=\frac{-\mathrm{i}\omega\cos(\lambda_l^S x/a)\cosh[m_1(y+h)]}{m_1\sinh[m_1(h-d)]}, \tag{2.38}$$

$$\tilde{\phi}_{lR}^{A(3)}(x,y)=\frac{-\mathrm{i}\omega\sin(\lambda_l^A x/a)\cosh[m_2(y+h)]}{m_2\sinh[m_2(h-d)]}, \tag{2.39}$$

where

$$m_1=((\lambda_l^S/a)^2+k_1^2\sin^2\theta)^{1/2},\quad m_2=((\lambda_l^A/a)^2+k_1^2\sin^2\theta)^{1/2}.$$

The unknown constants in equations (2.34) and (2.35) can be determined in a similar manner to the diffraction problem using the matching conditions at $x=-a$. The simultaneous algebraic equations for the unknown constants $a_{lm}^{S,A}$ in region (I) are given by

$$a_{lm}^{S,A}+\sum_{k=0}^{\infty}\frac{F_{mk}^{S,A}}{\alpha_{1m}N_m^{(1)}}a_{lk}^{S,A}=\frac{X_{ml}^{S,A}}{\alpha_{1m}N_m^{(1)}}\quad(m=0,1,2,3,\ldots), \tag{2.40}$$

where

$$X_{ml}^{S,A}=\frac{\mathrm{i}\omega}{g}\int_{-d}^{0}\frac{\partial\tilde{\phi}_{lR}^{S,A(2)}(-a,y)}{\partial x}f_{1m}(y)\,\mathrm{d}y+\int_{-h}^{-d}\frac{\partial\tilde{\phi}_{lR}^{S,A(3)}(-a,y)}{\partial x}f_{1m}(y)\,\mathrm{d}y\ . \tag{2.41}$$

The other unknown coefficients can be determined from

$$b_{ln}^{S}=\frac{\sum_{k=0}^{\infty}a_{lk}^{S}C_{nk}}{\cosh(\alpha_{2n}a)\,N_n^{(2)}},\quad c_{ln}^{S}=\frac{\sum_{k=0}^{\infty}a_{lk}^{S}D_{nk}}{\cosh(\alpha_{3n}a)\,N_n^{(3)}},\quad n\geqslant 0 \tag{2.42a}$$

and

$$b_{ln}^{A}=\frac{-\sum_{k=0}^{\infty}a_{lk}^{A}C_{nk}}{\sinh(\alpha_{2n}a)\,N_n^{(2)}},\quad c_{ln}^{A}=\frac{-\sum_{k=0}^{\infty}a_{lk}^{A}D_{nk}}{\sinh(\alpha_{3n}a)\,N_n^{(3)}},\quad n\geqslant 0. \tag{2.42b}$$

2.3. *Membrane response*

Neglecting viscous (or material) damping, the motion of the membrane is governed by the inhomogeneous one-dimensional wave equation as follows:

$$T\frac{\mathrm{d}^2\xi}{\mathrm{d}x^2}+m\omega^2\xi=-\mathrm{i}\rho\omega[\phi^{(3)}(x,-d)-\phi^{(2)}(x,-d)], \tag{2.43}$$

where T, ρ, and m are the membrane tension, fluid density, and membrane mass per unit length, respectively. Substituting

$$\phi(x,y)=\phi_D(x,y)+\sum_{j=1}^{\infty}\varsigma_j\phi_{jR}(x,y),\quad \xi(x)=\sum_{j=1}^{\infty}\varsigma_j f_j(x)$$

into (2.43) yields

$$\sum_{j=1}^{\infty}\varsigma_j\ -T\frac{\mathrm{d}^2 f_j(x)}{\mathrm{d}x^2}-m\omega^2 f_j(x)-p_{jR}(x)\ =p_D(x), \tag{2.44a}$$

where

$$p_{jR}(x)=\mathrm{i}\rho\omega[\phi_{jR}^{(3)}(x,-d)-\phi_{jR}^{(2)}(x,-d)],\quad p_D(x)=\mathrm{i}\rho\omega[\phi_D^{(3)}(x,-d)-\phi_D^{(2)}(x,-d)]. \tag{2.44b}$$

Multiplying (2.44a) by $f_i(x)$ and integrating over the membrane, we obtain

$$\sum_{j=1}^{\infty}\{K_{ij}-\omega^2(M_{ij}+\hat{a}_{ij})-\mathrm{i}\omega\hat{b}_{ij}\}\varsigma_j=F_i,\quad i=1,2,3,\ldots, \tag{2.45a}$$

where

$$\left.\begin{aligned} K_{ij}&=-\int_{-a}^{a}T\frac{\mathrm{d}^2 f_j(x)}{\mathrm{d}x^2}f_i(x)\,\mathrm{d}x,\quad M_{ij}=\int_{-a}^{a}mf_j(x)f_i(x)\,\mathrm{d}x,\\ \hat{a}_{ij}&=\mathrm{Re}\ \frac{1}{\omega^2}\int_{-a}^{a}p_{jR}(x)f_i(x)\,\mathrm{d}x\ ,\quad \hat{b}_{ij}=\mathrm{Im}\ \frac{1}{\omega}\int_{-a}^{a}p_{jR}(x)f_i(x)\,\mathrm{d}x\ ,\\ F_i&=\int_{-a}^{a}p_D(x)f_i(x)\,\mathrm{d}x. \end{aligned}\right\} \tag{2.45b}$$

The symbols K_{ij}, M_{ij}, and F_i represent the generalized (modal) stiffness matrix, mass matrix and force vector, respectively, and $\hat{a}_{ij}$ and $\hat{b}_{ij}$ are the generalized added-mass and radiation-damping tensors. Truncating the series of (2.45a) at the appropriate term M, we can solve for the unknown complex amplitudes ς_j corresponding to each mode. When the membrane is on the free surface, a hydrostatic correction term needs to be added (Newman 1994).

Finally, the reflection and transmission coefficients can be determined from

$$\left.\begin{aligned} R_f&=\ (a_0^S+a_0^A)+\sum_{l=1}^{M}\varsigma_l(a_{lR}^S+a_{lR}^A)\ \mathrm{e}^{\alpha_{10}a}\ ,\\ T_r&=\ (a_0^S-a_0^A)+\sum_{l=1}^{M}\varsigma_l(a_{lR}^S-a_{lR}^A)\ \mathrm{e}^{\alpha_{10}a}\ . \end{aligned}\right\} \tag{2.46}$$

The vertical hydrodynamic forces on the horizontal membrane can be calculated from

$$F=-\mathrm{i}\rho\omega\int_{-a}^{a}[\phi^{(3)}(x,-d)-\phi^{(2)}(x,-d)]\,\mathrm{d}x. \tag{2.47}$$

3. Numerical method

In this section, a numerical method based on a boundary integral equation is developed to confirm the analytic solutions described in the preceding section. The fluid domain is decomposed into two regions, inner and outer, as shown in figure 1(*b*).

The far-field solution is expressed by the expansion of the eigenfunctions (e.g. see the first equation of (2.15*a*)) which satisfy the modified Helmholtz equation, and free-surface, bottom, and radiation boundary conditions. The inner domain is divided into two sub-regions, as shown in figure 1(*b*). The inner solution in region I satisfies the boundary value problem given by equation (2.2)–(2.4) and the following boundary condition on the membrane:

$$\left.\frac{\partial\phi}{\partial y}\right|_{y=-d\pm 0} = -\mathrm{i}\omega\xi \quad \text{on} \quad -a \leqslant x \leqslant a. \tag{3.1}$$

On the other hand, the inner solution in region II satisfies the bottom condition and (3.1). In addition, the inner solutions are to be matched at the respective matching boundaries $\Gamma_{a\pm}$ and $\Gamma_{\pm}$. The velocity potential in the inner region can be obtained by applying Green's theorem with a Green function $\hat{G}$. The resulting integral equation is given by

$$\begin{matrix}\phi(x,y)\\ \frac{1}{2}\phi(x,y)\end{matrix} = \int_{\Gamma} \phi\frac{\partial\hat{G}}{\partial n} - \hat{G}\frac{\partial\phi}{\partial n}\,\mathrm{d}S \quad \begin{matrix}\text{if} \quad (x,y)\in\Omega \quad \text{but not on } \Gamma\\ \text{if} \quad (x,y) \quad \text{on} \quad \Gamma\end{matrix}, \tag{3.2}$$

where the Green function $\hat{G}$ is the fundamental solution satisfying

$$\nabla^2\hat{G} - k_1^2\sin^2\theta\hat{G} = -\delta(x-x_0)\,\delta(y-y_0),$$

and given by

$$G(x,y;x_0,y_0) = \frac{1}{2\pi}K_0(k_1\sin\theta r), \quad r = [(x-x_0)^2+(y-y_0)^2]^{1/2}, \tag{3.3}$$

where r is the distance between source point (x,y) and field point (x_0,y_0) and K_0 is the second-kind modified Bessel function of zeroth order. The normal derivative of $\hat{G}$ can also be obtained analytically in terms of K_1. To convert the above integral equation to a matrix equation, the entire boundary of the inner region is discretized by N elements, and the values of ϕ and $\partial\phi/\partial n$ are assumed to be constant over each element. Since the simple source K_0 is used, the bottom topography of the inner region can be arbitrary. Substituting the boundary conditions of region I into (3.2), the following equation is obtained:

$$\sum \left(H^{ij} - \frac{\omega^2}{g}G^{ij}\right)\phi_j^{(1)}|_{\Gamma_F} + \sum H^{ij}\phi_j^{(1)}|_{\Gamma_{\pm}} + \sum H^{ij}\phi_j^{(1)}|_{\Gamma_{b1}} + \sum H^{ij}\phi_j^{(1)}|_{\Gamma_{a\pm}} + \sum H^{ij}\phi_j^{(1)}|_{\Gamma_S}$$
$$-\sum \mathrm{i}\omega G^{ij}\xi_j|_{\Gamma_S} = \sum G^{ij}\left.\frac{\partial\phi_j^{(1)}}{\partial n}\right|_{\Gamma_{\pm}} + \sum G^{ij}\left.\frac{\partial\phi_j^{(1)}}{\partial n}\right|_{\Gamma_{a\pm}} \tag{3.4}$$

where ξ_j is the motion amplitude of the membrane and Γ_F, $\Gamma_{\pm}$, Γ_{b1}, $\Gamma_{a\pm}$, Γ_S are the free surface, matching boundary I (with the outer region), bottom surface, matching boundary II (with region II), and membrane surface, respectively. The influence coefficient H^{ij} and G^{ij} are defined by

$$H^{ij} = \int_{\Gamma_j}\frac{\partial G}{\partial n}\mathrm{d}S, \quad G^{ij} = \int_{\Gamma_j} G\,\mathrm{d}S. \tag{3.5}$$

Similarly, substituting the boundary conditions of region (II) into (3.2), we obtain

$$\sum H^{ij}\phi_j^{(2)}|_{\Gamma_S} + \sum \mathrm{i}\omega G^{ij}\xi_j|_{\Gamma_S} + \sum H^{ij}\phi_j^{(2)}|_{\Gamma_{a\pm}} + \sum H^{ij}\phi_j^{(2)}\left.\right|_{\Gamma_{b2}} = \sum G^{ij}\left.\frac{\partial\phi_j^{(2)}}{\partial n}\right|_{\Gamma_{a\pm}}. \tag{3.6}$$

At the matching boundary $\Gamma_{a\pm}$, the pressure and normal velocity must be continuous

$$\frac{\partial\bar{\phi}}{\partial n}=\frac{\partial\phi^{(1)}}{\partial n}=-\frac{\partial\phi^{(2)}}{\partial n},\quad \bar{\phi}=\phi^{(1)}=\phi^{(2)}\quad\text{at}\quad \Gamma_{a\pm}, \tag{3.6}$$

where the overbar means the value newly defined at the matching boundary $\Gamma_{a\pm}$.

On the membrane surface, the following dynamic condition has to be satisfied:

$$\frac{\mathrm{d}^2\xi}{\mathrm{d}x^2}+\lambda^2\xi+\mathrm{i}\omega\frac{c_d}{T}\xi=-\frac{\mathrm{i}\rho\omega}{T}[\phi^{(2)}(x,-d)-\phi^{(1)}(x,-d)] \tag{3.8}$$

in which $\lambda=\omega(m/T)^{1/2}$ with T and m being the membrane tension and mass per unit length, respectively, and c_d the linearized damping coefficient. Here, it is assumed that the initial tension T is large so that the effects of dynamic tension can be neglected. To transform the membrane equation into a discretized form, we divided the membrane surface into N_S elements with ξ representing the displacement of the centre point:

$$\mathrm{i}\rho\omega(\phi_j^{(2)}-\phi_j^{(1)})\,\Delta x_j-T\frac{(\xi_j-\xi_{j-1})}{\Delta x_j^m}+T\frac{(\xi_{j+1}-\xi_j)}{\Delta x_{j+1}^m}=-(m\omega^2+\mathrm{i}\omega c_d)\,\Delta x_j\,\xi_j, \tag{3.9}$$

where Δx_j is the length of the jth segment, and $\Delta x_j^m=(\Delta x_{j-1}+\Delta x_j)/2$. The above equation can be changed into a matrix form

$$\boldsymbol{\xi}=\boldsymbol{\Xi}(\boldsymbol{\phi}^{(2)}-\boldsymbol{\phi}^{(1)})|_{\Gamma_S} \tag{3.10}$$

where $\boldsymbol{\Xi}$ is an $N_S\times N_S$ matrix. Substituting (3.7) and (3.10) into (3.4) and (3.6), we obtain the following matrix equations:

$$\boldsymbol{H}-\frac{\omega^2}{g}\boldsymbol{G}\;\;\boldsymbol{\phi}^{(1)}|_{\Gamma_F}+\boldsymbol{H}\boldsymbol{\phi}^{(1)}|_{\Gamma_\pm}+\boldsymbol{H}\boldsymbol{\phi}^{(1)}|_{\Gamma_{b1}}+\boldsymbol{H}\bar{\boldsymbol{\phi}}|\Gamma_{a\pm}$$

$$+(\boldsymbol{H}+\mathrm{i}\omega\boldsymbol{G}\boldsymbol{\Xi})\boldsymbol{\phi}^{(1)}|_{\Gamma_S}-\mathrm{i}\omega\boldsymbol{G}\boldsymbol{\Xi}\boldsymbol{\phi}^{(2)}|_{\Gamma_S}-\boldsymbol{G}\frac{\partial\bar{\boldsymbol{\phi}}}{\partial n}_{\Gamma_{a\pm}}-\boldsymbol{G}\frac{\partial\boldsymbol{\phi}^{(1)}}{\partial n}_{\Gamma_\pm}=0 \tag{3.11}$$

$$-\mathrm{i}\omega\boldsymbol{G}\boldsymbol{\Xi}\boldsymbol{\phi}^{(1)}|_{\Gamma_S}+\boldsymbol{H}\bar{\boldsymbol{\phi}}|_{\Gamma_{a\pm}}+(\boldsymbol{H}+\mathrm{i}\omega\boldsymbol{G}\boldsymbol{\Xi})\,\boldsymbol{\phi}^{(2)}|_{\Gamma_S}+\boldsymbol{H}\boldsymbol{\phi}^{(2)}|_{\Gamma_{b2}}+\boldsymbol{G}\frac{\partial\bar{\boldsymbol{\phi}}}{\partial n}_{\Gamma_{a\pm}}=0. \tag{3.12}$$

By applying a remaining matching condition (continuity of pressure and normal velocity) between the far field solution and the inner solution I at $\Gamma_\pm$, a final matrix equation can be derived and the unknown coefficients of the outer solution can be determined.

When a membrane is located on the free surface, a simpler two-domain approach can be used using only a single inner solution. When the system is submerged, however, the inner domain should be separated into two subregions since the membrane is infinitely thin.

4. Experiments

In order to validate the theory and numerical procedure developed in the preceding section, we conducted a series of experiments in the two-dimensional wave tank (37 m

	Experiment no. 1	Experiment no. 2	Experiment no. 3
Membrane length (cm)	80	80	80
Membrane width (cm)	82	82	82
Submembrane depth (cm)	16	16	0
Water depth (cm)	80	80	56
Membrane tension (kg F)	36	21	36
Wave frequency (Hz)	0.5–1.4	0.5–1.4	0.5–1.4
Wave amplitude (cm)	3, 4, 5	3	3

TABLE 1. Experimental conditions

long, 0.91 m wide, and 1.22 m deep) located at Texas A & M University. The glass-walled wave tank is equipped with a dry-back, hinged-flap wave maker capable of producing regular and irregular waves.

The wave elevation was measured with resistance wave gauges that have an accuracy of ± 0.1 cm. A probe measuring incident and reflected wave heights and another probe measuring the transmitted wave heights are placed 9.1 m and 22.9 m from the wavenumber, respectively. The wave barrier model was placed 18.3 m from the wavemaker between the two probes (see figure 1 *c*). Regular waves were generated by a user-defined time-voltage input to the wave maker. The wave frequency range used in our experiments was from 0.5 to 1.4 Hz. The wave heights used were 6, 8 and 10 cm. The time series of the regular wave packet generated was sinusoidal with the beginning and end of the series attenuated in amplitude.

The model membrane ($m = 0.17$ kg m^{-2}) was made of a thin stretch-resistible plastic material resembling a plastic tarpaulin. The length and width of the membrane were 80 and 82 cm, respectively. The ends of the membrane were attached to two horizontal steel bars which are fixed by four vertical steel frames clamped to the tank, as shown in figure 1 (*c*). The tension on the membrane was provided by a series of string-weight units. The end-bar of the tensioned membrane was then fixed to a new location of the steel frame. After the tension is correctly given, the string-weight units were removed. Table 1 summarizes the principal characteristics of the models and wave conditions used in the experiments.

The signal of the incident wave train is obtained as it passes the probe toward the membrane breakwater. Then, the reflected wave train is recorded as the reflected waves pass the probe again in the opposite direction. After averaging the wave heights for the incident, reflected, and transmitted wave trains, the reflection coefficient R_f and transmission coefficient T_r can be calculated from the ratio of the averaged reflected and transmitted wave height to the averaged incident wave height. During the experiments, we observed that reflected and transmitted waves were repeatedly reflected from the wave maker and beach. In order to minimize the effects of multiple reflection, the present method was adopted in favour of the moving-single probe method or three-probe method (Isaacson 1991) which require a relatively longer time to establish a steady state. It is shown in Hagan (1994) that the present method is more reliable than the moving- or three-probe methods when nonlinear phenomena or multiple reflections exist. In most of our experiments, the errors estimated from the energy relation were kept within 10 %. The discrepancy can be attributed to viscous, gap, and nonlinear effects, and membrane material damping, etc. When the membrane is located on or very close to the calm water level, the energy-conservation error is increased due to wave overtopping the membrane.

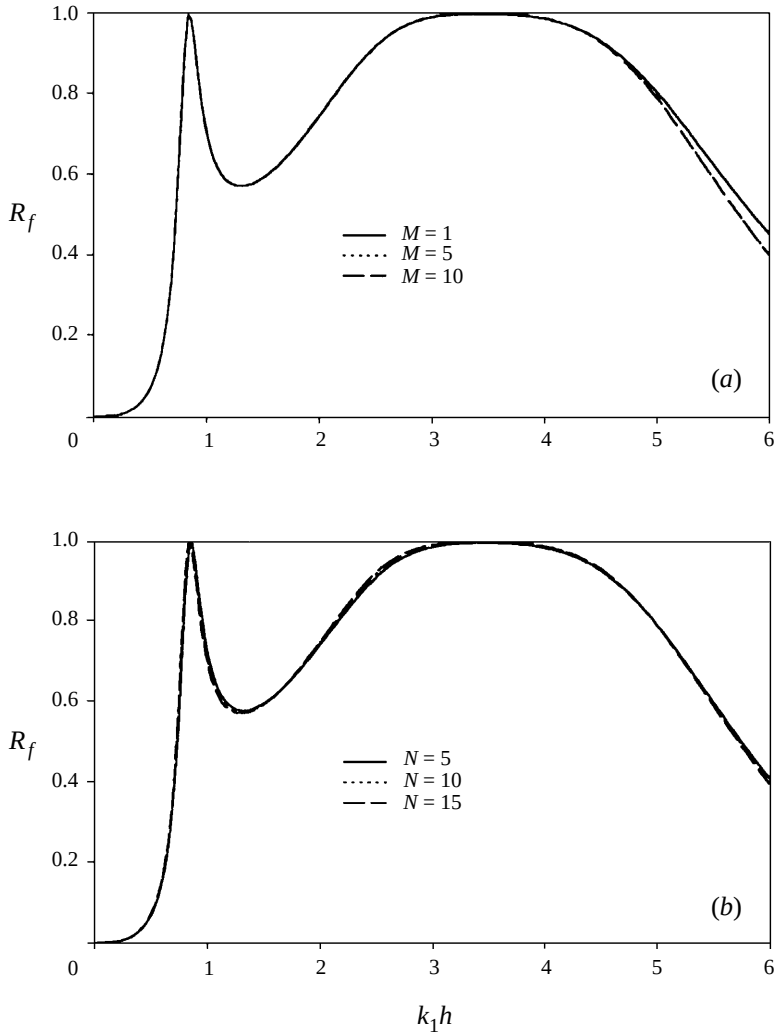

FIGURE 2. Convergence of reflection coefficient with (*a*) the number of natural modes of the membrane for $N = 10$ (N = number of eigenfunctions); and (*b*) the number of eigenfunctions for $M = 5$. $d/h = 0.2$, $a/h = 0.5$, $T/\rho g h^2 = 0.1$, $\theta = 0°$.

$M \diagdown N$	5	10	20	40	60
1	0.4617	0.4566	0.4517	0.4486	0.4475
5	0.4137	0.4049	0.3981	0.3941	0.3927
10	0.4136	0.4046	0.3981	0.3941	0.3927

TABLE 2. Convergence test for the case of figure 2 at $k_1 h = 6$

5. Results and discussion

The analytic solutions described in §2 were compared with the BEM-based numerical solutions explained in §3. First, the convergence of analytic solutions with the number of natural modes M and eigenfunctions N is shown in figure 2. A more

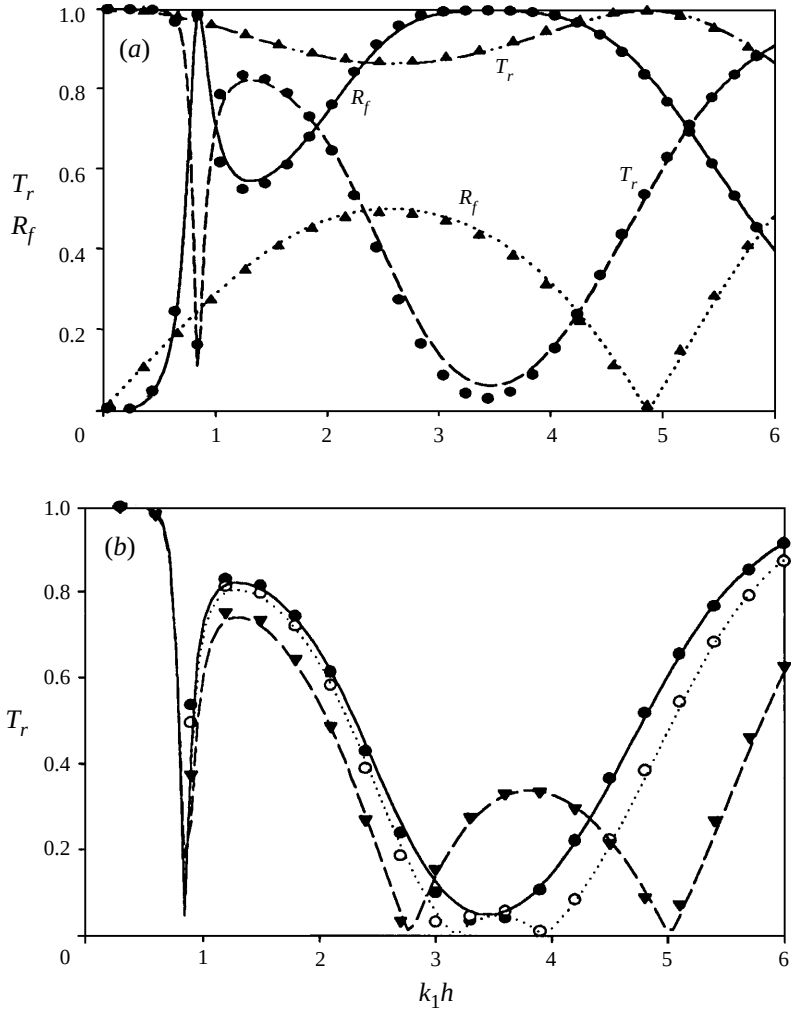

FIGURE 3. Reflection and transmission coefficient of a submerged ($d = 0.2h$, ——, ●; – – – –, ●) and floating ($d = 0$, ------; ▲; – – – –, ▲) horizontal membrane breakwater as function of non-dimensional wavenumber $k_1 h$ for $a/h = 0.5$, $T/\rho g h^2 = 0.1$, and $\theta = 0°$. Lines are for analytic solutions and symbols are for BEM solutions. (*b*) Transmission coefficients of a submerged horizontal membrane breakwater as function of non-dimensional wavenumber $k_1 h$ for $d/h = 0.2$, $a/h = 0.5$, $T/\rho g h^2 = 0.1$; ——, ●, $\theta = 0°$, ------, ○, $\theta = 15°$, – – –, ▼, $\theta = 30°$. (Lines, analytic solutions, symbols, BEM solutions).

detailed convergence-test result for $k_1 h = 6$ can be seen in table 2. It is seen that the convergence with M is faster than that with N and results with 1% error can be obtained with $M = 5$, $N = 10$. Next, the analytic solutions with $M = 5$, $N = 10$ are compared in figure 3(*a*) with the BEM solutions. For the BEM result, 500 total elements for the submerged membrane and 200 total elements for the surface-mounted membrane were used. More elements were used for the submerged membrane case due to more computational domains and boundaries, as explained in §3. The two solutions are in good agreement in both submerged and surface-mounted cases. The two results also agree well in the case of oblique incidence waves and converge uniformly toward the normal-incidence results as the wave angle approaches zero, as can be seen in figure

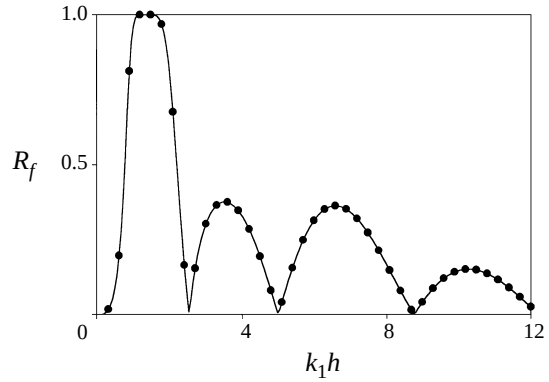

FIGURE 4. Comparison of the infinite-tension case (——) with McIver's rigid-plate result (●) ($a/h = 0.5$, $d/h = 0.1$).

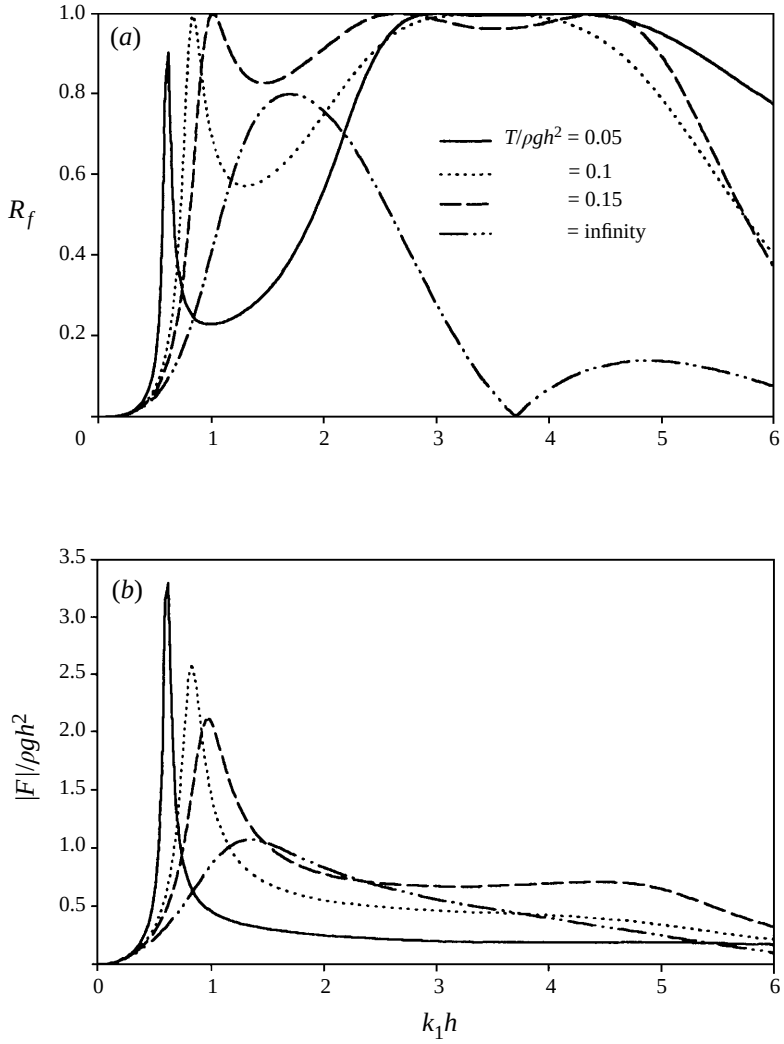

FIGURE 5. (*a*) Reflection coefficient and (*b*) hydrodynamic loading of a submerged horizontal membrane breakwater as function of non-dimensional tension $T/\rho gh^2$ and wavenumber $k_1 h$ for $d/h = 0.2$, $a/h = 0.5$, and $\theta = 0°$.

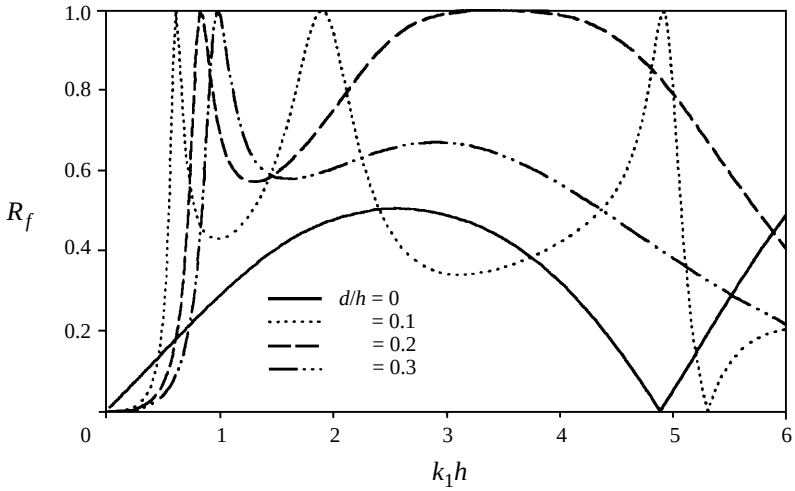

FIGURE 6. Reflection coefficient of a submerged impermeable membrane breakwater as function of submergence depth d/h and wavenumber $k_1 h$ for $a/h = 0.5$, $T/\rho g h^2 = 0.1$, and $\theta = 0°$.

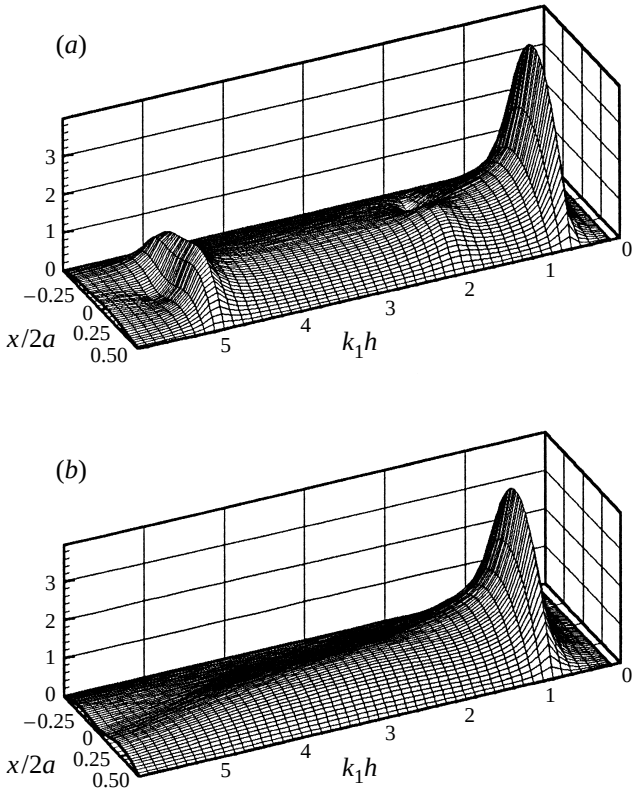

FIGURE 7. Responses of a membrane ($|\xi|/A$) as a function of wavenumber $k_1 h$ and horizontal coordinate $x/2a$ for (*a*) $d/h = 0.1$, and (*b*) 0.2 ($a/h = 0.5$, $T/\rho g h^2 = 0.1$, and $\theta = 0°$).

3(*b*). In addition, both analytic and numerical solutions were checked against the energy relation $R_f^2 + T_r^2 = 1$. The infinite-tension case corresponds to the diffraction by a rigid horizontal plate which was studied by McIver (1985) for the normal-incidence

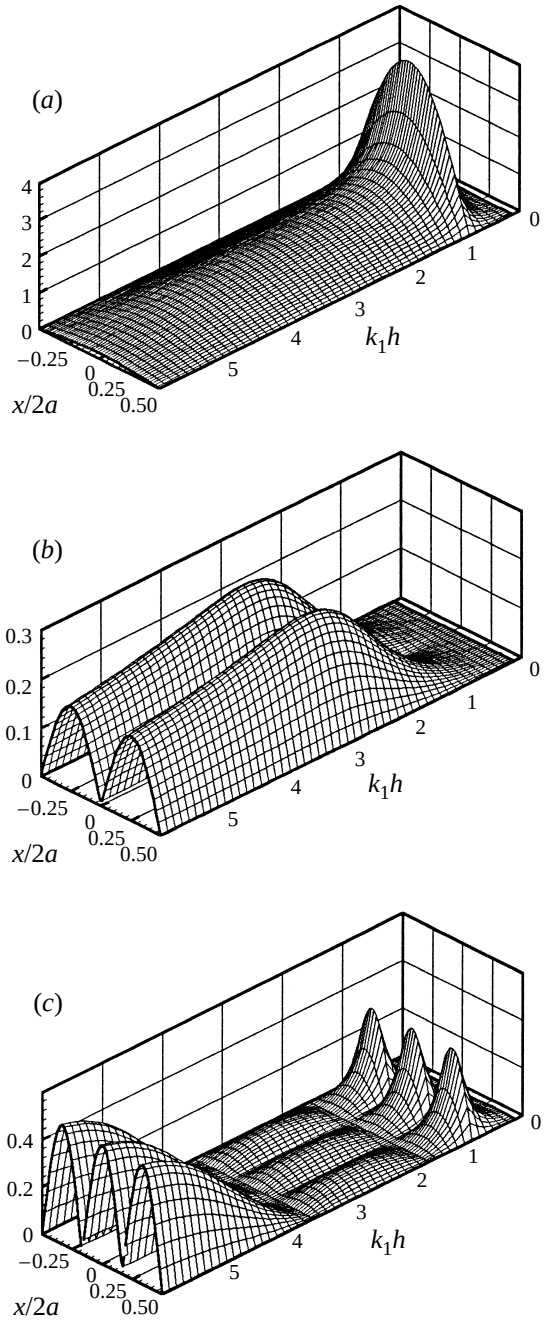

FIGURE 8. Model response amplitude as function of wavenumber $k_1 h$ and horizontal coordinate $x/2a$ for $d/h = 0.2$, $a/h = 0.5$, $T/\rho g h^2 = 0.1$, and $\theta = 0°$. (*a*) First mode, (*b*) second mode, (*c*) third mode.

case. The correctness of the limiting case was checked against McIver's results, as can be seen in figure 4. In the following, the analytic solutions with $M = 5$, $N = 10$ were used to investigate the performance of a horizontal flexible membrane wave barrier for various design conditions. The membrane mass per unit length used for these numerical examples was 1 kg m^{-2}.

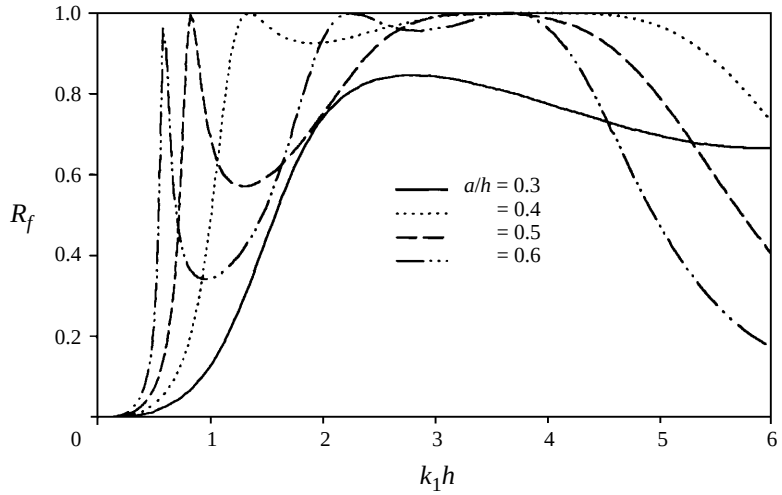

FIGURE 9. Reflection coefficients of a submerged impermeable membrane breakwater as function of length of membrane a/h and wavenumber $k_1 h$ for $d/h = 0.2$, $T/\rho g h^2 = 0.1$, and $\theta = 0°$.

In figures 5(*a*) and 5(*b*) the reflection coefficients by and hydrodynamic loading on a particular horizontal membrane are plotted for various membrane tensions. It is seen that flexible membranes generally perform better than rigid plates (infinite tension) and there exists an optimal tension for the given design condition. In figure 5(*b*) the hydrodynamic loading for the lower tension (or more flexible membrane) tends to be smaller but has a larger and narrower peak near the resonance region.

In figure 6, the membrane tension (T) and length ($2a$) are fixed and the submergence depth (d) is varied from 0 to 0.3 h. For this example, the overall efficiency is best for the case $d = 0.2h$. The trend of the limiting case $d = 0$ (membrane on the calm water surface) is quite different from that of the other curves because only the lower part of the surface-mounted membrane is exposed to the fluid loading. In figure 7, the amplitudes of membrane responses (normalized by incident wave amplitude) are plotted for the cases $d = 0.1h$ and $0.2h$ as a function of dimensionless x-coordinate and wavenumbers. It is interesting to see that the performance is good when membrane motions are not small, which indicates that the motion-induced waves in this case tend to reduce the transmitted waves through phase cancellation. As a reference, the modal amplitudes of each mode (normalized by incident wave amplitude) are plotted in figure 8 for the case $d = 0.2h$. It is shown that the model amplitudes of higher harmonics are rapidly decreased. The higher harmonics become relatively more important at higher $k_1 h$ values.

In the next figure (figure 9), the membrane tension and submergence depth are fixed and the size (length) of membrane is varied from $a = 0.3h$ to $0.6h$. Interestingly, the bandwidth of the high-performance region is largest when $a = 0.4h$, which implies that the efficiency is not necessarily improved with the larger size of membrane. However, the non-zero reflection region can be extended to longer waves by increasing the size of membrane.

We next plot in figure 10(*a*) the reflection coefficients of a horizontal membrane with the different incident wave headings. We can see that the efficiency for oblique waves can increase or decrease compared to the normal-incidence case depending on the wave frequencies. Interestingly, the performance in the long-wave regime $k_1 h < 1$ is little

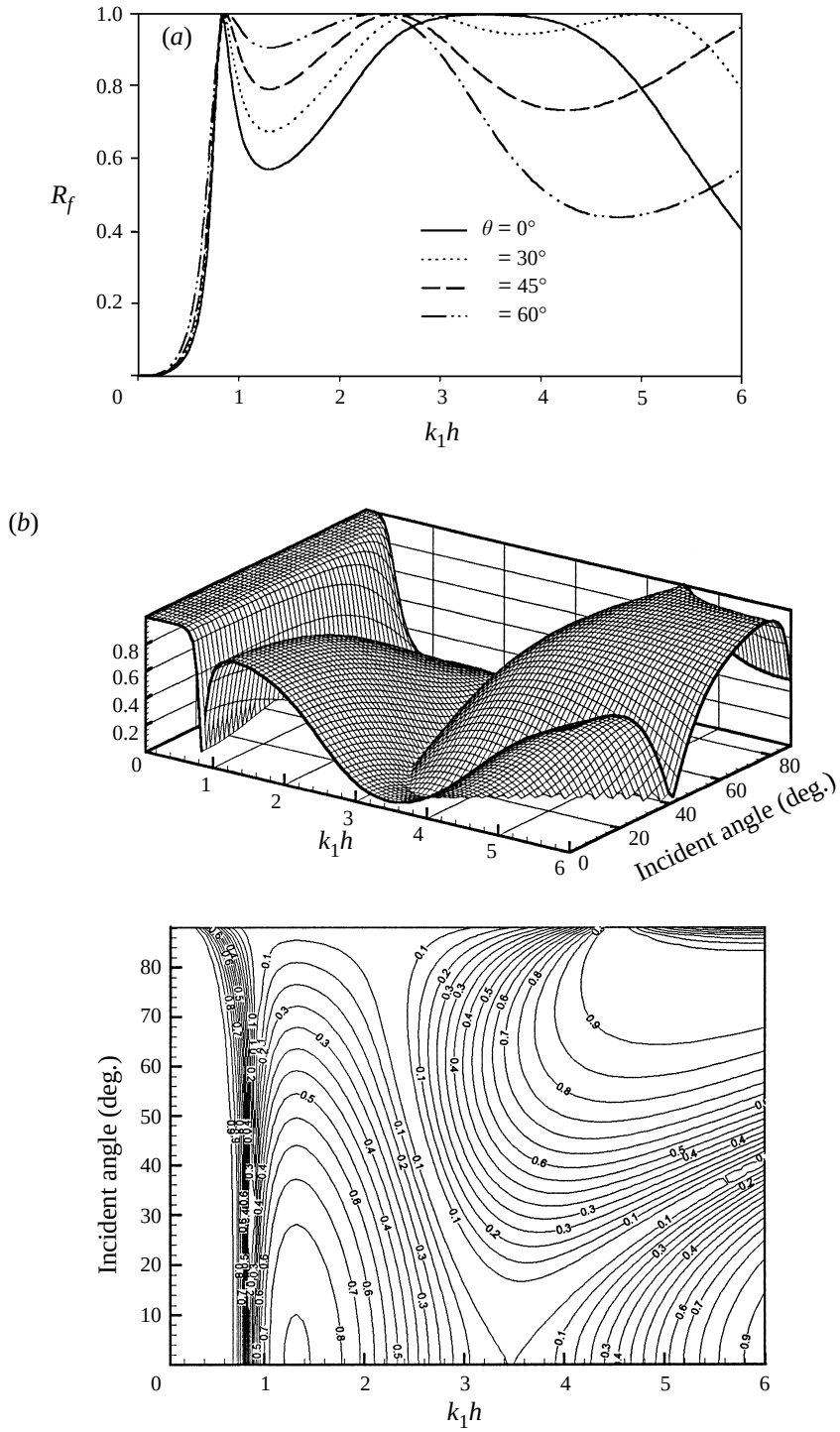

FIGURE 10. (*a*) Reflection coefficients of a submerged impermeable membrane breakwater as function of incident heading angle θ and wavenumber $k_1 h$ for $d/h = 0.2$, $a/h = 0.5$, and $T/\rho g h^2 = 0.1$. (*b*) Three-dimensional and contour plots of T_r for the case shown in (*a*).

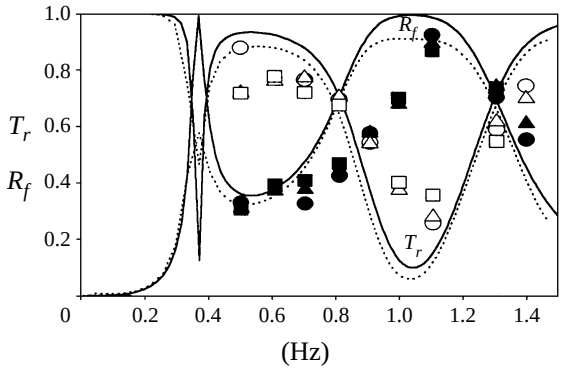

FIGURE 11. Comparison of analytic results with measured values (exp. 1) for a submerged horizontal membrane breakwater; analytic solutions without damping (——) and with damping (------); experimental results R_f (filled symbols) and T_r (open symbols) (circle: wave amplitude = 3 cm, triangle: 4 cm, square: 5 cm).

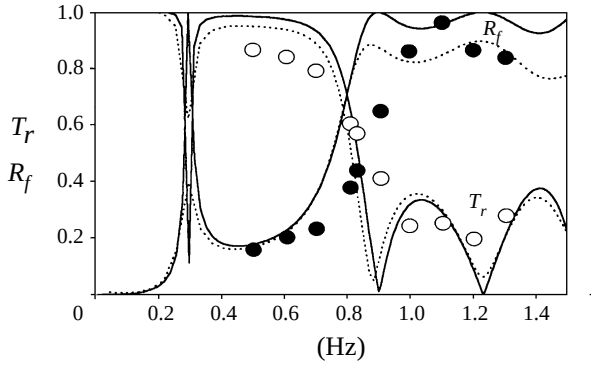

FIGURE 12. Comparison of analytic results with measured values (exp. 2) for a submerged horizontal membrane breakwater; analytic solution without damping (——) and with damping (------); experimental results R_f (filled symbols) and T_r (open symbols).

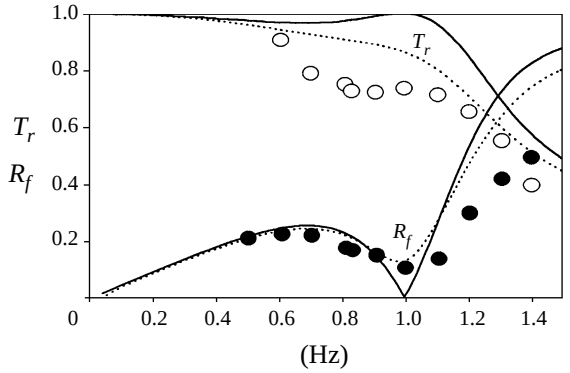

FIGURE 13. Comparison of analytic results with measured values (exp. 3) for a floating horizontal membrane breakwater; analytic solution without damping (——) and with damping (------); experimental results R_f (filled symbols) and T_r (open symbols).

influenced by the change of incident angles. Figure 10(*b*) shows the corresponding three-dimensional and contour plots for transmission coefficients.

Finally, the computational results for several designs are compared with the experimental results conducted in the two-dimensional wave tank located at Texas A & M University. The measured values generally follow the trend of the computed curves. The same experiment was conducted for three different incident wave amplitudes, and the general trend looks similar. It can be seen in figure 11 that the wave blocking performance is indeed good in the range $0.8 < f < 1.3$ Hz, as predicted by the present linear hydro-elastic theory. In the same figure, we also show the effects of viscous (or material) damping (10 % damping ratio) on membrane motions. For the estimation of the damping ratio, a linear damping coefficient is assumed and the first-mode added mass was used to calculate the virtual modal mass. We can notice that its effect is the largest near the resonance region ($f \approx 0.35$ Hz). The discrepancy between the predicted and measured results can be attributed to the uncertainties in the amount of viscous (or material) damping, nonlinear effects, gap or end effects, etc. In particular, we observed during the experiment that the membrane response was not perfectly uniform in the z-direction mainly due to end effects. Figure 12 shows similar comparisons for smaller membrane tension. Again, the measured values generally follow the predicted values. The wave blocking efficiency in this case is very good when $f > 0.8$ Hz and near $f \approx 0.3$ Hz. The next figure (figure 13) shows similar comparisons for the surface-mounted membrane. The performance of this design is not good unless $f > 1.2$ Hz. For this particular case, the wave overtopping the surface-mounted membrane adds more uncertainty with regard to the validity of the present theoretical model. Despite the additional uncertainty, the trend of experimental values follows reasonably that of predicted values.

6. Summary and conclusions

The interaction of oblique monochromatic incident waves with a horizontal flexible membrane was investigated in the context of two-dimensional linear hydro-elastic theory. In §2, analytic diffraction and radiation solutions for a submerged horizontal membrane were obtained for arbitrary incident wave angles by matching the eigenfunction solutions in the three fluid domains. The analytic solutions were confirmed by independently developed numerical solutions, which used a discrete membrane dynamic model and simple-source (second-kind modified Bessel function) distribution method. The theoretical prediction was then compared with a series of experiments conducted with a stretch-resistible horizontal membrane and reasonable agreement was obtained.

Using the computer program developed, the performance of surface-mounted or submerged horizontal membrane wave barriers was tested with various membrane tensions, lengths, and submergence depths. Since the horizontal membrane does not directly block incoming waves, the transmitted and motion-induced waves need to be properly cancelled for it to be an effective wave barrier. It was seen that an optimal combination of design parameters existed for given water depths and wave characteristics. The efficiency can be further enhanced and the motions reduced by using a porous membrane, which will be the subject of future study.

From the present study, it can be concluded that a properly designed horizontal flexible membrane can be a very effective wave barrier and its optimal design can be found through a comprehensive parametric study using the theory and computer

programs developed. For further verification, a more rigorous nonlinear time-domain numerical analysis and larger-scale experiments need to be done.

This research was sponsored by the Korea Research Institute of Ships & Ocean Engineering (KRISO) through KRISO/TAMU cooperative research program. This work was also partly supported by the Offshore Technology Research Center through the National Science Foundation Engineering Research Centers Program, Grant Number CDR-8721512.

REFERENCES

Abul-Azm, A. G. 1994 Wave diffraction by double flexible breakwaters. *J. Appl. Ocean Res.* **16**, 87–99.

Aoki, S., Liu, H. & Sawaragi, T. 1994 Wave transformation and wave forces on submerged vertical membrane. *Proc. Intl Symp. Waves – Physical and Numerical Modeling*, *Vancouver*, pp. 1287–1296.

Dean, R. G. & Dalrymple, R. A. 1991 *Water Wave Mechanics for Engineers and Scientists*. World Scientific.

Hagan, C. L. 1994 A theoretical/experimental study of a perforated wall wave absorber. MS thesis, Texas A & M University, College Station.

Isaacson, M. 1991 Measurement of regular wave. *ASCE J. Waterway*, *Port*, *Coastal Ocean Engng* **117**, 553–569.

Kee, S. T. & Kim, M. H. 1997 Flexible membrane wave barrier. Part 2. Floating/submerged buoy-membrane system. *ASCE J. Waterway*, *Port*, *Coastal Ocean Engng* **123**, 82–90.

Kim, M. H., Edge, B. L., Kee, S. T. & Zhang, L. 1966 Performance evaluation of buoy-membrane wave barriers. *Proc. 25th Intl Conf. on Coastal Engineering*, *Orlando*, *Florida*.

Kim, M. H. & Kee, S. T. 1996 Flexible membrane wave barrier. Part 1. Analytic and numerical solutions. *ASCE J. Waterway*, *Port*, *Coastal Ocean Engng* **122**, 46–53.

Lee, J. F. & Chen, C. J. 1990 Wave interaction with hinged flexible breakwater. *J. Hydraul. Res.* **28**, 283–295.

McIver, M. 1985 Diffraction of water waves by a moored, horizontal, flat plate. *J. Engng Maths* **19**, 297–320.

Newman, J. N. 1994 Wave effects on deformable bodies. *J. Appl. Ocean Res.* **16**, 47–59.

Siew, P. F. & Hurley, D. G. 1977 Long surface waves incident on a submerged horizontal plate. *J. Fluid Mech.* **83**, 141–151.

Thompson, G. O., Sollitt, C. K., McDougal, W. G. & Bender, W. R. 1992 Flexible membrane wave barrier. *ASCE Conf. Ocean V*, College Station, pp. 129–148.

Williams, A. N., Geiger, P. T. & McDougal, W. G. 1991 Flexible floating breakwater. *ASCE J. Waterway*, *Port*, *Coastal Ocean Engng* **117**, 429–450.

Williams, A. N. 1996 Floating membrane breakwater. *J. Offshore Mechanics Arctic Engng* **118**, 46–51.